Tuning electronic properties of silicane layers by tensile strain and external electric field: A first-principles study

Sake Wang, Jin Yu

PII: S0040-6090(18)30205-0
DOI: doi:10.1016/j.tsf.2018.03.061
Reference: TSF 36565

To appear in: *Thin Solid Films*

Received date: 2 August 2017
Revised date: 12 March 2018
Accepted date: 20 March 2018

Please cite this article as: Sake Wang, Jin Yu , Tuning electronic properties of silicane layers by tensile strain and external electric field: A first-principles study. The address for the corresponding author was captured as affiliation for all authors. Please check if appropriate. Tsf(2017), doi:10.1016/j.tsf.2018.03.061

Tuning electronic properties of silicane layers by tensile strain and external electric field: A first-principles study

Sake Wang[a,*], Jin Yu[b]

a Department of Fundamental Courses, Jinling Institute of Technology, Nanjing 211169, China

b School of Materials Science and Engineering, Southeast University, Nanjing 211189, China

Abstract

The structural and electronic properties of silicane layers and bulk, the effects of a biaxial tensile strain and an external electric field (E-field) on the electronic properties of silicane monolayer and bilayer are investigated using density functional theory computations with the van der Waals (vdW) correction. It is demonstrated that the weak vdW interaction between silicane layers can efficiently tune the electronic properties of silicane multilayers. The silicane multilayers (up to 5) are indirect bandgap semiconductors whose bandgap slightly decreases with the number of layers, whereas bulk silicane is a direct bandgap semiconductor. The bandgaps of both silicane monolayer and bilayer can be flexibly modulated by applying a biaxial tensile strain, and indirect-direct transition occurs when the biaxial tensile strain reaches +4% and +2%, respectively. Besides, the bandgaps of the silicane monolayer and bilayer can also be continuously modulated by an external E-field, with an indirect-direct transition observed when its magnitude reaches 0.5 and 0.7 V/Å, respectively. A larger E-field can trigger a semiconductor-metal transition at approximately 0.8 V/Å for both silicane monolayer and bilayer. Our results provide rather effective and flexible approaches to tune the electronic properties of silicane layers for application in silicane-based electronic and optoelectronic devices.

1. Introduction

Silicene [1,2], the silicon analog of graphene, is a two-dimensional (2D) crystal with a hexagonal lattice structure. A number of experiments have realized the epitaxial growth of silicene on some metal substrates, such as Ag [1–7], Ir [8] and ZrB_2 thin films [9]. As reported by early theoretical works, silicene is a zero-bandgap semimetal, similar to graphene. Silicene also exhibits linear energy dispersion behavior around the Fermi level at the *K* point, which can lead to high carrier mobility [1,10]. Some fantastic features, such as a quantum spin Hall effect [11,12], giant magnetoresistance [13] and multiple topological interface states [14] have been predicted for monolayer silicene. Despite its outstanding electronic properties and effective integration with current silicon-based microelectronics, silicene cannot be used in many fields, such as field-effect transistors (FETs), because its zero bandgap restricts the achievability of on-off current ratio. Hence, some effective strategies should be adopted to open a bandgap in silicene.

Doping [15–24], adsorption [25–29] and functionalization [30,31] are three effective approaches to tuning the electronic and magnetic properties of 2D materials. For silicene, chemical functionalization [32–47] is a pretty effective technique for tuning its properties. For instance, the electronic and magnetic properties of silicene can be well tuned by half-hydrogenation, as reported by many theoretical [41,42] and experimental works [43,44]. An extreme example, which had previously been investigated by many theoretical works [40,45,46] is silicane (fully hydrogenated silicene). It is an indirect semiconductor with a bandgap of 2.94 eV (by Heyd-Scuseria-Ernzerhof (HSE06)) [47]. Potential applications such as high-performance FET [48], optoelectronic devices [49] and even

* E-mail: IsaacWang@jit.edu.cn

hydrogen storage [50] have been proposed for this promising 2D material. Considering the controllable bandgap engineering of semiconductors is an essential part of nanoelectronics and optoelectronics, a comprehensive investigation on modulating the electronic properties of silicane is of great interest and critical to widen the range of its applications.

Recently, the weak van der Waals (vdW)-like coupling between layers, such as in graphane [51], germanane [52], phosphorene [53–55], transition metal dichalcogenides [56–58], and many vertical heterostructures [59–69] has been well investigated. For example, Fokin et al. [51] computationally demonstrated that graphane can form multi-layered structures similar to graphene due to the weak vdW interaction, which is really dumbfounding because it was believed that all the bonds in graphane are fully saturated so that it can hardly form vdW interaction between two monolayers [70]. Li et al. [52] demonstrated correspondingly that there exists the weak vdW interaction between germanane layers. The interactions between these layers play an important role in bandgap engineering. These intensive studies on the weak vdW-like interaction between layers inspired us to answer a motivating question: How does this interaction affect the electronic properties of silicane layer? Moreover, can we efficiently modulate the electronic properties of silicane layers by some feasible approaches?

In this article, we present a systematic investigation of the structural and electronic properties of silicane layers by using vdW-corrected density functional theory (DFT) computations. Our calculations reveal that there is the weak vdW interaction between silicane layers. Silicane multilayers inherit the indirect bandgap characteristic of the silicane monolayer. Significantly, the bandgaps of the silicane monolayer and bilayer can be constantly modulated by a biaxial tensile strain and an external electric field (E-field), so that an indirect-direct bandgap transition can be triggered. Our investigations could pave the way for applications of such few-layered silicane in FETs with a high on-off current ratio and optoelectronic devices functioning under visible light.

2. Calculation methods

First-principles calculations are implemented by the Vienna *ab initio* Simulation Package (VASP) [71–73], which uses a projector augmented wave [74] formalism. The generalized gradient approximation for the exchange-correlation functional of the Perdew-Burke-Ernzerhof (PBE) [75,76] form is employed. The vdW correction proposed by Grimme (DFT-D2) [77] is chosen to describe the weak interactions. It is relatively well-known that Generalized Gradient Approximation (GGA) constantly leads to an underestimation of the bandgap of semiconductor. To tackle this issue, calculations based on the HSE hybrid functional [78–81] were also performed simultaneously for many critical results. The energy cutoff is taken to be 550 eV. In order to avoid interactions between adjacent layers, a vacuum region of 20 Å in *z* direction has been sandwiched. The Brillouin zone is sampled using a 21 × 21 × 1 Monkhorst-Pack [82] grid. All the structures are fully relaxed until the Hellmann-Feynman forces are less than 0.01 eV/Å.

3. Results and discussion

3.1 Structural and electronic properties of the silicane multilayers

Fig. 1(a) depicts the optimized geometric structure of a silicane monolayer in a 4 × 4 supercell. The most stable form of the silicane layer favors a chair-like conformation with hydrogen adatoms alternately adsorbed on two sides of the layer, structurally like graphane [83]. The system belongs to $P6_3mc$ group with C_{3v} symmetry. The optimized lattice parameter, Si-Si bond length, Si-H bond length and buckling height are 3.89, 2.36, 1.50 and 0.72 Å, respectively, which are consistent with previously reported results [84–86]. Computed with the PBE functional, the silicane monolayer is semiconducting with an indirect bandgap of 2.19 eV (see Fig. 1(b)), and it is smaller than the HSE06

functional result, 2.94 eV (see Fig. A.1(a) in Appendix). The conduction band minimum (CBM) and valence band maximum (VBM) of the silicane monolayer are located at the *M* and *Γ* points respectively (see Fig. 1(b)). The partial charge density of CBM and VBM of silicane monolayer is analyzed, as shown in Fig. 1(c). The CBM is mainly contributed by the Si-H σ* anti-bonding state of H s and Si s p_z orbitals while the VBM is dominated by the Si p_x orbitals.

The silicane bilayer can be formed by stacking two silicane monolayers together. To obtain the most stable structure of the silicane bilayer, we consider four logical structures (see Fig. 2). Generally, the binding energies for these structures are in the range of 61 to 103 meV/unit-cell.

The most stable structure of the silicane bilayer (see Fig. 3(a)) has two Si skeletons in AA stacking, and the H atom of the bottom layer points straightly to the Si atom of the upper layer with an interlayer Si-H distance of 3.30 Å, and the average H-H bond length is 2.48 Å. Denis et al. [39] also showed that the most stable structure of the silicane bilayer has AA stacking previously, even though they used a different code. However, Li et al. [52] revealed that the lowest-energy structure of the germanane bilayer addresses an AB stacking. They performed the computations using the DMol^3 code [87,88]. We examined the favorite structure of the germanane bilayer energetically by using VASP code and found results in agreement with those of Li et al. [52]. Therefore, it is obvious that the lowest-energy structure of the silicane bilayer is different from the situation of the germanane bilayer.

In addition to the DFT-D2 method, we also tested the performance of the untouched PBE method for describing the layer interaction in silicane bilayer systems. The PBE approach gives a vanishingly small binding energy of 8 meV and a very long H-H bond length of 3.11 Å. These results are quite different from those of the DFT-D2 approach. Moreover, the total energy of the four silicane bilayer structure predicted by the PBE method is almost equal (with an energy difference of less than 2 meV). Thus, PBE is incapable of describing the interaction between the two silicane layers. These results also demonstrate great usefulness of the DFT-D2 approach in describing weak interactions.

Next, we move on to explore the electronic structure of the silicane bilayer. The band structure calculated by PBE functional for the most stable structure of the silicane bilayer is shown in Fig. 3(b), while the one calculated by HSE functional is shown in the Fig. A.1(b) in Appendix. When two monolayers are piled to form a bilayer, we found an indirect bandgap of 2.09 eV and 2.83 eV using the PBE and HSE functionals respectively, which are slightly smaller than the values for a silicane monolayer (2.19 and 2.94 eV respectively).

Since the energy difference between the four silicane bilayer structures is relatively small (no more than 41 meV), we also investigated the band structures of the other three metastable structures (see Fig. 2). These structures also exhibit indirect semiconducting behavior. The bandgaps vary from 2.12 to 2.17 eV (using the PBE functional), slightly larger than the most stable one (2.09 eV).

We next explored the band structure of silicane multilayers with a layer number up to 5 and three-dimensional bulk silicane (see Fig. 4), which can be seen as the extreme case of silicane multilayers. Interestingly, in stark contrast to phosphorene (bulk black phosphorus is an indirect bandgap material but transforms to a direct bandgap semiconductor when thinned to a monolayer) [89], silicane is an indirect bandgap material in its few-layer form but a direct bandgap semiconductor in its bulk form. The bandgaps were 2.04, 2.03, 2.01 and 2.03 eV for trilayer, tetralayer, pentalayer and bulk silicane respectively. Calculations based on the HSE06 functional also showed that bulk silicane is a direct bandgap semiconductor with an energy gap of 2.81 eV (see Fig. A.2 in Appendix). In parallel, the energy differences between the indirect and direct bandgaps (that is also the energy differences

between the first and second conduction band) were approximately 0.22, 0.10, 0.07, 0.05, 0.04 and -0.11 eV for monolayer, bilayer, trilayer, tetralayer, pentalayer and bulk silicane respectively. As the layer number increases, the difference becomes smaller. Hence, although the vdW interaction between silicane layers is rather weak, this type of weak interaction can still fine-tune the electronic properties of multilayer silicane systems. It is straightforward to conclude that these systems have potential applications in nanoelectronics, such as in FETs with a high on-off current ratio. Silicane in its bulk form in particular can have potential applications for optoelectronic devices functioning under visible light.

3.2 Modulation of the band structure via biaxial tensile strain

Applying tensile strain has proven to be a very efficient method of modulating the electronic and magnetic properties of 2D materials [49,90,91]. Recently, Shu et al. [49] predicted an indirect-direct bandgap transition in a silicane monolayer under a strain of 2.74%. Hence, can we effectively modulate the band structure of a silicane bilayer to induce an indirect-direct bandgap transition?

To answer this question, we first calculated the band structure of a silicane monolayer under a biaxial tensile strain (see Fig. 5(a)). In accordance with the previous investigation [49], we found an indirect-direct bandgap transition under a strain of approximately 4%. Then, we investigated the band structure of a silicane bilayer under a biaxial tensile strain. We find an indirect-direct bandgap transition under a strain of 2% from Fig. 5(b). The direct bandgap occurs at the Γ point. It is significant that both the silicane monolayer and bilayer perseveres with direct-gap semiconductors for a very wide range of strain with values up to 10%. These are considerably important results from the application point of view since the direct-gap semiconducting behavior is vital for optoelectronic applications.

The dependence of the bandgap of silicane monolayer and bilayer on the biaxial tensile strain is depicted in Fig. 6. For a silicane monolayer, with a biaxial tensile strain, the bandgap increases at first and reaches a maximum value (2.23 eV) at approximately 2%, and then decreases monotonically with a further increase of strain. However, for a silicane bilayer, the bandgap decreases almost monotonically with the increase of strain. Moreover, the response of the bandgap of the silicane bilayer to biaxial tensile strain is more sensitive than the monolayer one. The trend is very similar to the case of germanane, where Li et al. [52] demonstrated that the bandgap of germanane monolayer and bilayer decreases with increasing biaxial tensile strain. We also computed the dependence of the bandgaps of silicane monolayer and bilayer on the biaxial tensile strain using the HSE06 functional (see Fig. A.3 in Appendix). Indeed, the GGA method usually underestimates the value of the bandgap. However, the general trends of the lines bear a strong likeness, so the trends predicted in Fig. 6 should be highly reliable. Therefore, we demonstrated that strain can dramatically tailor the bandgaps of silicane monolayer and bilayer and can thereby be used to modulate the bandgap of silicane in nanoelectronic and optoelectronic applications.

3.3 Effect of an external E-field

An external E-field is a powerful tool for directly tuning the electronic properties of 2D materials [92–95]. For instance, a widely tunable bandgap can be achieved in graphene bilayer by applying an external E-field [92]. Li et al. [93] demonstrated that by applying an external E-field up to 15 V/nm, the bandgap of pristine or deformed phosphorene can be continuously modulated and finally closed. The bandgap versus the external E-field for a silicane monolayer and a silicane bilayer is plotted in Fig. 7. Due to the existence of the inversion symmetry along the *z* direction in the silicane monolayer and bilayer, we have performed calculations with the strength of the external E-field ranging from 0 to 1.0 V/Å.

As shown in Fig. 7, for a silicane monolayer, its bandgap is rather robust under an external E-field strength up to 0.4 V/Å. However, at an E-field of 0.5 V/Å, it exhibits a direct gap with both the CBM and VBM at the Γ point (see Fig. 8(a)). If we further increase the strength to 0.6 V/Å, the bandgap is significantly reduced while the direct bandgap feature is sustained. When the strength of the E-field increases to 0.8 V/Å, a semiconductor-metal transition occurs. Further increase in the E-field does not change the metallic behavior of the silicane monolayer. We also computed the electronic structure of a silicane monolayer under an E-field by employing the HSE06 functional (see Fig. A.4 in Appendix). Indeed, we obtained much larger bandgaps than those using the PBE functional. However, the trend should be reliable and the HSE06 functional only increases the critical value of the E-field (0.9 V/Å) for the semiconductor-metal transition. For a silicane bilayer, the bandgap decreases sharply as the strength of the external E-field increases. Similarly, an E-field of 0.7 V/Å gives a direct gap with both the CBM and VBM at the Γ point (see Fig. 6(b)). We also observed a semiconductor-metal transition like in the silicane monolayer when the field reaches 0.9 V/Å. For a larger E-field, the system remains metallic. Once again, the HSE06 results confirm the trend of the field-modulated bandgap (see Fig. A.4 in Appendix).

Conclusion

The structural and electronic properties of silicane layers and bulk, the effects of an external E-field on the electronic properties of silicane monolayer and bilayer are thoroughly investigated using DFT computations with the vdW correction. We found the following to be true: (i) The most stable structure of the silicane bilayer has AA stacking and is characterized by the weak vdW interaction between two adjacent layers. (ii) The bandgaps of few-layer (up to 5) silicane are all indirect, and the bandgap slightly decreases with the number of layers. (iii) The indirect-direct bandgap transition can be triggered in both silicane monolayer and bilayer by a tensile strain and an external E-field. Overall, our investigation provides three effective approaches, namely, weak vdW interaction, tensile strain and external E-field, for tailoring the electronic properties of silicane layers, and offering great possibilities for the applications of silicane in electronic and optoelectronic devices.

Acknowledgement

This work was supported by the National Science Foundation for Young Scientists of China [grant number 11704165]; the Science Foundation of Guizhou Science and Technology Department [grant number QKHJZ(2015)2150]; the Science Foundation of Guizhou Provincial Education Department [grant number QJHKYZ(2016)092]; as well as the Science Foundation of Jinling Institute of Technology [grant number 40620064].

Appendix

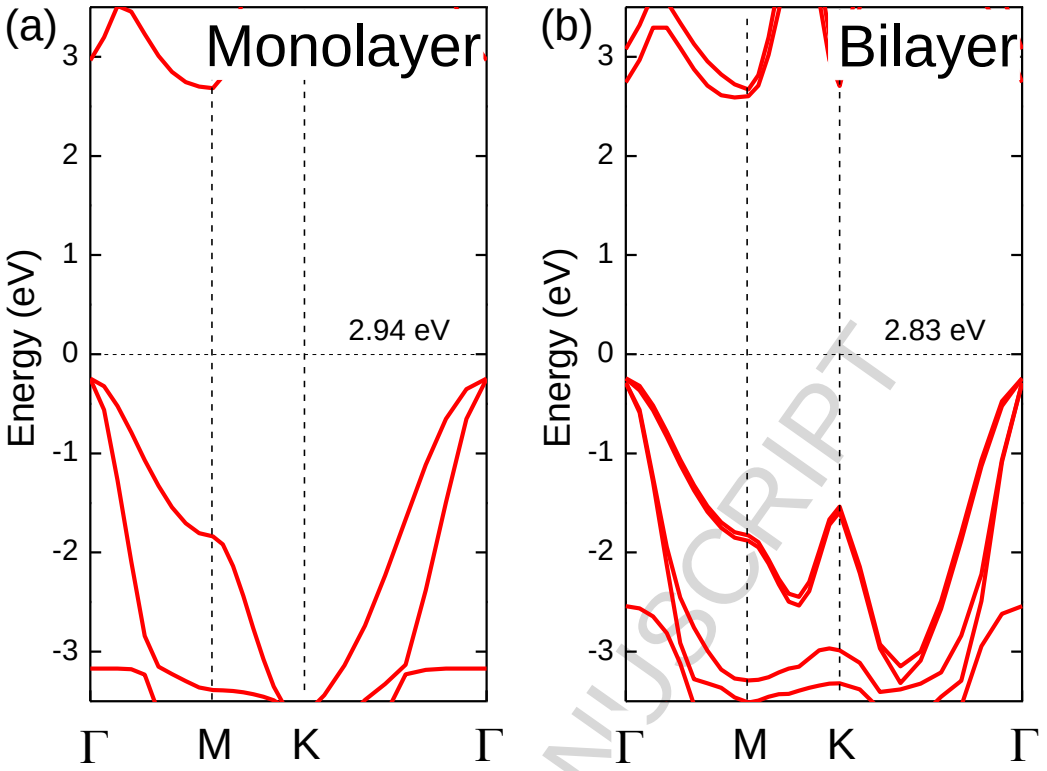

Fig. A.1 Electronic band structure of (a) silicane monolayer and (b) silicane bilayer computed using HSE06 functional. The zero energy value corresponds to the Fermi level.

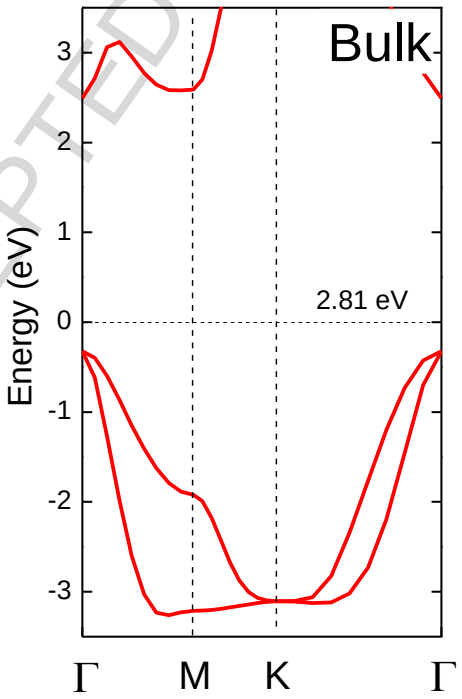

Fig. A.2 Electronic band structure of bulk silicane computed using HSE functional. The zero energy value corresponds to the Fermi level.

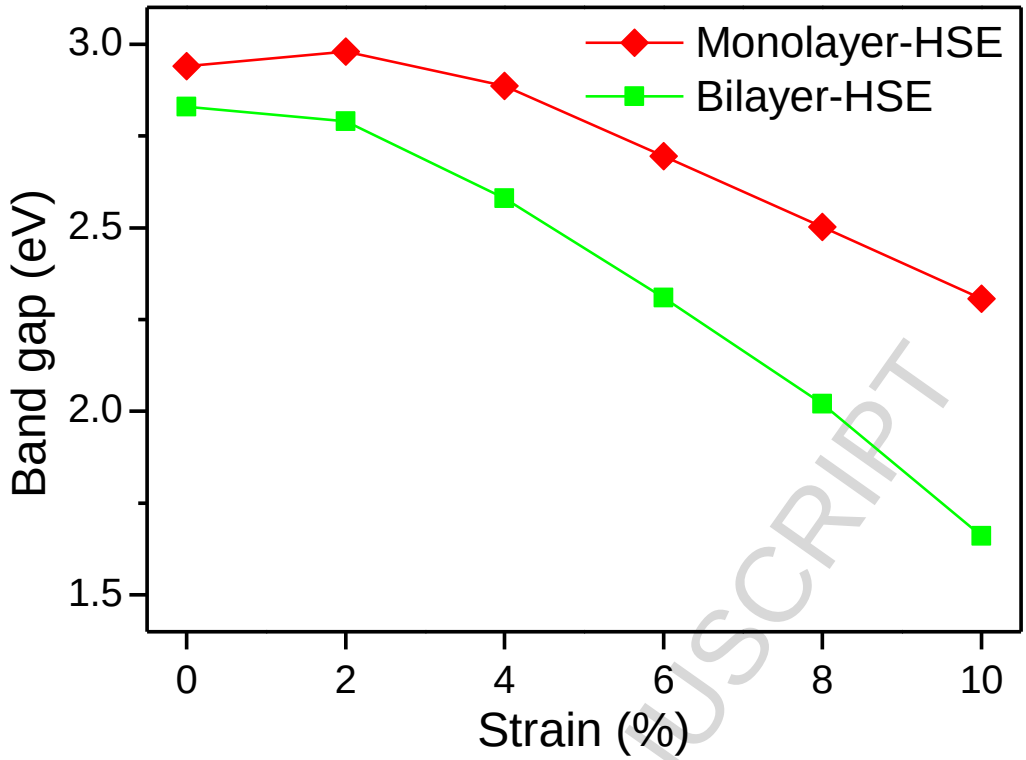

Fig. A.3 Energy bandgap of silicane monolayer and bilayer as a function of the biaxial tensile strain computed using HSE06 functional.

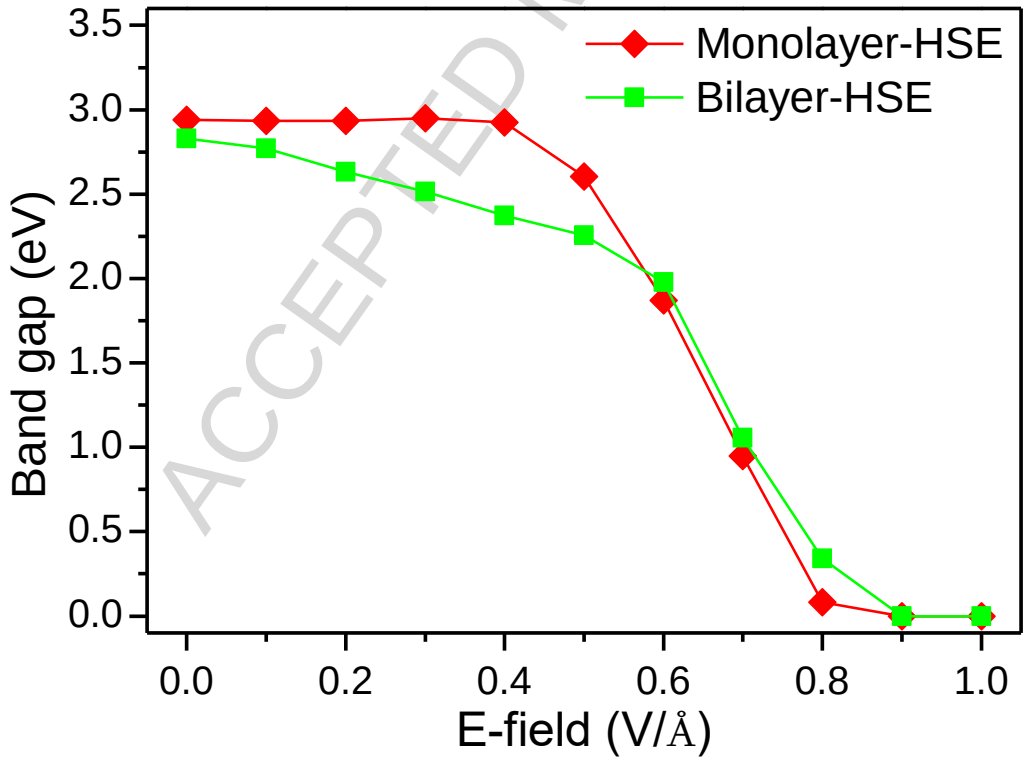

Fig. A.4 Energy bandgap of silicane monolayer and bilayer as a function of the external E-field computed using HSE06 functional.

References

[1] S. Cahangirov, M. Topsakal, E. Aktürk, H. Şahin, S. Ciraci, Two- and one-dimensional honeycomb structures of silicon and germanium, Phys. Rev. Lett. 102 (2009) 236804.

[2] P. Vogt, P. de Padova, C. Quaresima, J. Avila, E. Frantzeskakis, M.C. Asensio, A. Resta, B. Ealet, G. Le Lay, Silicene: compelling experimental evidence for graphenelike two-dimensional silicon, Phys. Rev. Lett. 108 (2012) 155501.

[3] C.-L. Lin, R. Arafune, K. Kawahara, N. Tsukahara, E. Minamitani, Y. Kim, N. Takagi, M. Kawai, Structure of silicene grown on Ag(111), Appl. Phys. Express 5 (2012) 45802.

[4] A. Resta, T. Leoni, C. Barth, A. Ranguis, C. Becker, T. Bruhn, P. Vogt, G. Le Lay, Atomic structures of silicene layers grown on Ag(111): scanning tunneling microscopy and noncontact atomic force microscopy observations, Sci. Rep. 3 (2013) 2399.

[5] A. Resta, T. Leoni, C. Barth, A. Ranguis, C. Becker, T. Bruhn, P. Vogt, G. Le Lay, Erratum: Atomic structures of silicene layers grown on Ag(111): scanning tunneling microscopy and noncontact atomic force microscopy observations, Sci. Rep. 3 (2013) 3298.

[6] B. Feng, Z. Ding, S. Meng, Y. Yao, X. He, P. Cheng, L. Chen, K. Wu, Evidence of silicene in honeycomb structures of silicon on Ag(111), Nano Lett. 12 (2012) 3507–3511.

[7] L. Chen, C.-C. Liu, B. Feng, X. He, P. Cheng, Z. Ding, S. Meng, Y. Yao, K. Wu, Evidence for Dirac fermions in a honeycomb lattice based on silicon, Phys. Rev. Lett. 109 (2012) 56804.

[8] L. Meng, Y. Wang, L. Zhang, S. Du, R. Wu, L. Li, Y. Zhang, G. Li, H. Zhou, W.A. Hofer, H.-J. Gao, Buckled silicene formation on Ir(111), Nano Lett. 13 (2013) 685–690.

[9] A. Fleurence, R. Friedlein, T. Ozaki, H. Kawai, Y. Wang, Y. Yamada-Takamura, Experimental evidence for epitaxial silicene on diboride thin films, Phys. Rev. Lett. 108 (2012) 245501.

[10] Z.-G. Shao, X.-S. Ye, L. Yang, C.-L. Wang, First-principles calculation of intrinsic carrier mobility of silicene, J. Appl. Phys. 114 (2013) 93712.

[11] M. Ezawa, Valley-polarized metals and quantum anomalous Hall effect in silicene, Phys. Rev. Lett. 109 (2012) 55502.

[12] C.-C. Liu, W. Feng, Y. Yao, Quantum spin Hall effect in silicene and two-dimensional germanium, Phys. Rev. Lett. 107 (2011) 76802.

[13] C. Xu, G. Luo, Q. Liu, J. Zheng, Z. Zhang, S. Nagase, Z. Gao, J. Lu, Giant magnetoresistance in silicene nanoribbons, Nanoscale 4 (2012) 3111–3117.

[14] S.K. Wang, J. Wang, K.S. Chan, Multiple topological interface states in silicene, New J. Phys. 16 (2014) 45015.

[15] M. Sun, Q. Ren, S. Wang, Y. Zhang, Y. Du, J. Yu, W. Tang, Magnetism in transition-metal-doped germanene: A first-principles study, Comput. Mater. Sci. 118 (2016) 112–116.

[16] N. Feng, W. Mi, Y. Cheng, Z. Guo, U. Schwingenschlögl, H. Bai, First principles prediction of the magnetic properties of Fe-X_6 (X = S, C, N, O, F) doped monolayer MoS_2, Sci. Rep. 4 (2014) 3987.

[17] M. Sun, Q. Ren, Y. Zhao, S. Wang, J. Yu, W. Tang, Magnetism in transition metal-substituted germanane: A search for room temperature spintronic devices, J. Appl. Phys. 119 (2016) 143904.

[18] M. Sun, S. Wang, Y. Du, J. Yu, W. Tang, Transition metal doped arsenene: A first-principles study, Appl. Surf. Sci. 389 (2016) 594–600.

[19] Y.C. Cheng, Z.Y. Zhu, W.B. Mi, Z.B. Guo, U. Schwingenschlögl, Prediction of two-dimensional diluted magnetic semiconductors: Doped monolayer MoS_2 systems, Phys. Rev. B 87 (2013) 100401.

[20] M. Sun, Y. Hao, Q. Ren, Y. Zhao, Y. Du, W. Tang, Tuning electronic and magnetic properties of blue phosphorene by doping Al, Si, As and Sb atom: A DFT calculation, Solid State Commun. 242 (2016) 36–40.

[21] M. Sun, W. Tang, Q. Ren, S.-k. Wang, J. Yu, Y. Du, A first-principles study of light non-metallic atom substituted blue phosphorene, Appl. Surf. Sci. 356 (2015) 110–114.

[22] E.J.G. Santos, A. Ayuela, D. Sánchez-Portal, First-principles study of substitutional metal impurities in graphene: structural, electronic and magnetic properties, New J. Phys. 12 (2010) 53012.

[23] M. Sun, W. Tang, Q. Ren, Y. Zhao, S. Wang, J. Yu, Y. Du, Y. Hao, Electronic and magnetic behaviors of graphene with 5d series transition metal atom substitutions: A first-principles study, Physica E: Low-dimens. Syst. Nanostruct. 80 (2016) 142–148.
[24] M. Sun, Q. Ren, Y. Zhao, J.-P. Chou, J. Yu, W. Tang, Electronic and magnetic properties of 4d series transition metal substituted graphene: A first-principles study, Carbon 120 (2017) 265–273.
[25] W. Tang, M. Sun, J. Yu, J.-P. Chou, Magnetism in non-metal atoms adsorbed graphene-like gallium nitride monolayers, Appl. Surf. Sci. 427 (2018) 609–612.
[26] Y. Ding, Y. Wang, Structural, electronic, and magnetic properties of adatom adsorptions on black and blue phosphorene: a first-principles study, J. Phys. Chem. C 119 (2015) 10610–10622.
[27] M. Sun, W. Tang, Q. Ren, S. Wang, J. Yu, Y. Du, Y. Zhang, First-principles study of the alkali earth metal atoms adsorption on graphene, Appl. Surf. Sci. 356 (2015) 668–673.
[28] K.T. Chan, J.B. Neaton, M.L. Cohen, First-principles study of metal adatom adsorption on graphene, Phys. Rev. B 77 (2008) 235430.
[29] S.K. Wang, J. Wang, Valley precession in graphene superlattices, Phys. Rev. B 92 (2015) 75419.
[30] M. Sun, S. Wang, J. Yu, W. Tang, Hydrogenated and halogenated blue phosphorene as Dirac materials: A first principles study, Appl. Surf. Sci. 392 (2017) 46–50.
[31] W. Tang, M. Sun, Q. Ren, S. Wang, J. Yu, Halogenated arsenenes as Dirac materials, Appl. Surf. Sci. 376 (2016) 286–289.
[32] Y. Wang, Y. Ding, Mechanical and electronic properties of stoichiometric silicene and germanene oxides from first-principles, Phys. Status Solidi RRL 7 (2013) 410–413.
[33] M. Sun, Q. Ren, S. Wang, J. Yu, W. Tang, Electronic properties of Janus silicene: new direct band gap semiconductors, J. Phys. D: Appl. Phys. 49 (2016) 445305.
[34] J.C. Garcia, D.B. de Lima, L.V.C. Assali, J.F. Justo, Group IV graphene- and graphane-like nanosheets, J. Phys. Chem. C 115 (2011) 13242–13246.
[35] M. Houssa, E. Scalise, K. Sankaran, G. Pourtois, V.V. Afanas'ev, A. Stesmans, Electronic properties of hydrogenated silicene and germanene, Appl. Phys. Lett. 98 (2011) 223107.
[36] N. Gao, W.T. Zheng, Q. Jiang, Density functional theory calculations for two-dimensional silicene with halogen functionalization, Phys. Chem. Chem. Phys. 14 (2012) 257–261.
[37] W.-B. Zhang, Z.-B. Song, L.-M. Dou, The tunable electronic structure and mechanical properties of halogenated silicene: a first-principles study, J. Mater. Chem. C 3 (2015) 3087–3094.
[38] W. Tang, M. Sun, Q. Ren, Y. Zhang, S. Wang, J. Yu, First principles study of silicene symmetrically and asymmetrically functionalized with halogen atoms, RSC Adv. 6 (2016) 95846–95854.
[39] P.A. Denis, Stacked functionalized silicene: a powerful system to adjust the electronic structure of silicene, Phys. Chem. Chem. Phys. 17 (2015) 5393–5402.
[40] Y. Ding, Y. Wang, Electronic structures of silicene fluoride and hydride, Appl. Phys. Lett. 100 (2012) 83102.
[41] X. Wang, H. Liu, S.-T. Tu, First-principles study of half-fluorinated silicene sheets, RSC Adv. 5 (2015) 6238–6245.
[42] C.-w. Zhang, S.-s. Yan, First-principles study of ferromagnetism in two-dimensional silicene with hydrogenation, J. Phys. Chem. C 116 (2012) 4163–4166.
[43] J. Qiu, H. Fu, Y. Xu, Q. Zhou, S. Meng, H. Li, L. Chen, K. Wu, From silicene to half-silicane by hydrogenation, ACS Nano 9 (2015) 11192–11199.
[44] W. Wang, W. Olovsson, R.I.G. Uhrberg, Band structure of hydrogenated silicene on Ag(111): Evidence for half-silicane, Phys. Rev. B 93 (2016) 81406.
[45] L.C. Lew Yan Voon, E. Sandberg, R.S. Aga, A.A. Farajian, Hydrogen compounds of group-IV nanosheets, Appl. Phys. Lett. 97 (2010) 163114.
[46] V. Zólyomi, J.R. Wallbank, V.I. Fal'ko, Silicane and germanane: tight-binding and first-principles studies, 2D Mater. 1 (2014) 11005.
[47] O.D. Restrepo, R. Mishra, J.E. Goldberger, W. Windl, Tunable gaps and enhanced mobilities in strain-engineered silicane, J. Appl. Phys. 115 (2014) 33711.
[48] K.L. Low, W. Huang, Y.C. Yeo, G. Liang, Ballistic transport performance of silicane and germanane transistors, IEEE T. Electron Dev. 61 (2014) 1590–1598.

[49] H. Shu, S. Wang, Y. Li, J. Yip, J. Wang, Tunable electronic and optical properties of monolayer silicane under tensile strain: A many-body study, J. Chem. Phys. 141 (2014) 64707.
[50] J. Wang, J. Li, S.-S. Li, Y. Liu, Hydrogen storage by metalized silicene and silicane, J. Appl. Phys. 114 (2013) 124309.
[51] A.A. Fokin, D. Gerbig, P.R. Schreiner, σ/σ- and π/π-interactions are equally important: multilayered graphanes, J. Am. Chem. Soc. 133 (2011) 20036–20039.
[52] Y. Li, Z. Chen, Tuning electronic properties of germanane layers by external electric field and biaxial tensile strain: a computational study, J. Phys. Chem. C 118 (2014) 1148–1154.
[53] S. Lei, H. Wang, L. Huang, Y.-Y. Sun, S. Zhang, Stacking fault enriching the electronic and transport properties of few-layer phosphorenes and black phosphorus, Nano Lett. 16 (2016) 1317–1322.
[54] J. Dai, X.C. Zeng, Bilayer phosphorene: effect of stacking order on bandgap and its potential applications in thin-film solar cells, J. Phys. Chem. Lett. 5 (2014) 1289–1293.
[55] Y. Cai, G. Zhang, Y.-W. Zhang, Layer-dependent band alignment and work function of few-layer phosphorene, Sci. Rep. 4 (2014) 6677.
[56] J. He, K. Hummer, C. Franchini, Stacking effects on the electronic and optical properties of bilayer transition metal dichalcogenides MoS_2, $MoSe_2$, WS_2, and WSe_2, Phys. Rev. B 89 (2014) 75409.
[57] H.-P. Komsa, A.V. Krasheninnikov, Electronic structures and optical properties of realistic transition metal dichalcogenide heterostructures from first principles, Phys. Rev. B 88 (2013) 85318.
[58] Q. Liu, L. Li, Y. Li, Z. Gao, Z. Chen, J. Lu, Tuning electronic structure of bilayer MoS_2 by vertical electric field: A first-principles investigation, J. Phys. Chem. C 116 (2012) 21556–21562.
[59] M. Sun, J.-P. Chou, Y. Zhao, J. Yu, W. Tang, Weak C-H···F-C hydrogen bonds make a big difference in graphane/fluorographane and fluorographene/fluorographane bilayers, Phys. Chem. Chem. Phys. 19 (2017) 28127–28132.
[60] Y. Song, D. Li, W. Mi, X. Wang, Y. Cheng, Electric field effects on spin splitting of two-dimensional van der Waals arsenene/$FeCl_2$ heterostructures, J. Phys. Chem. C 120 (2016) 5613–5618.
[61] Q. Yang, C.-J. Tan, R.-S. Meng, J.-K. Jiang, Q.-H. Liang, X. Sun, D.-G. Yang, X. Chen, AlN/BP heterostructure photocatalyst for water splitting, IEEE Electron Device Lett. 38 (2017) 145–148.
[62] J. Jiang, Q. Liang, S. Zhang, R. Meng, C. Tan, Q. Yang, X. Sun, H. Ye, X. Chen, Tuning the electronic and optical properties of graphane/silicane and fhBN/silicane nanosheets *via* interfacial dihydrogen bonding and electrical field control, J. Mater. Chem. C 4 (2016) 8962–8972.
[63] C. Tan, Q. Yang, R. Meng, Q. Liang, J. Jiang, X. Sun, H. Ye, X.P. Chen, An AlAs/germanene heterostructure with tunable electronic and optical properties *via* external electric field and strain, J. Mater. Chem. C 4 (2016) 8171–8178.
[64] M. Sun, J.-P. Chou, J. Yu, W. Tang, Effects of structural imperfection on the electronic properties of graphene/WSe_2 heterostructures, J. Mater. Chem. C 5 (2017) 10383–10390.
[65] Y. Wang, Y. Ding, The electronic structures of group-V-group-IV hetero-bilayer structures: a first-principles study, Phys. Chem. Chem. Phys. 17 (2015) 27769–27776.
[66] M. Sun, J.-P. Chou, Q. Ren, Y. Zhao, J. Yu, W. Tang, Tunable Schottky barrier in van der Waals heterostructures of graphene and g-GaN, Appl. Phys. Lett. 110 (2017) 173105.
[67] Y. Cai, G. Zhang, Y.-W. Zhang, Electronic properties of phosphorene/graphene and phosphorene/hexagonal boron nitride heterostructures, J. Phys. Chem. C 119 (2015) 13929–13936.
[68] B. You, X. Wang, Z. Zheng, W. Mi, Black phosphorene/monolayer transition-metal dichalcogenides as two dimensional van der Waals heterostructures: a first-principles study, Phys. Chem. Chem. Phys. 18 (2016) 7381–7388.
[69] M. Sun, J.-P. Chou, J. Yu, W. Tang, Electronic properties of blue phosphorene/graphene and blue phosphorene/graphene-like gallium nitride heterostructures, Phys. Chem. Chem. Phys. 19 (2017) 17324–17330.
[70] J.O. Sofo, A.S. Chaudhari, G.D. Barber, Graphane: A two-dimensional hydrocarbon, Phys. Rev. B 75 (2007) 153401.

[71] G. Kresse, J. Furthmüller, Efficient iterative schemes for ab initio total-energy calculations using a plane-wave basis set, Phys. Rev. B 54 (1996) 11169–11186.
[72] G. Kresse, J. Furthmüller, Efficiency of ab-initio total energy calculations for metals and semiconductors using a plane-wave basis set, Comput. Mater. Sci. 6 (1996) 15–50.
[73] G. Kresse, J. Hafner, Ab initio molecular dynamics for liquid metals, Phys. Rev. B 47 (1993) 558–561.
[74] G. Kresse, D. Joubert, From ultrasoft pseudopotentials to the projector augmented-wave method, Phys. Rev. B 59 (1999) 1758–1775.
[75] J.P. Perdew, K. Burke, M. Ernzerhof, Generalized gradient approximation made simple, Phys. Rev. Lett. 77 (1996) 3865–3868.
[76] J.P. Perdew, K. Burke, M. Ernzerhof, Generalized gradient approximation made simple [Phys. Rev. Lett. 77, 3865 (1996)], Phys. Rev. Lett. 78 (1997) 1396.
[77] S. Grimme, Semiempirical GGA-type density functional constructed with a long-range dispersion correction, J. Comput. Chem. 27 (2006) 1787–1799.
[78] J. Paier, M. Marsman, K. Hummer, G. Kresse, I.C. Gerber, J.G. Ángyán, Screened hybrid density functionals applied to solids, J. Chem. Phys. 124 (2006) 154709.
[79] J. Paier, M. Marsman, K. Hummer, G. Kresse, I.C. Gerber, J.G. Ángyán, Erratum: "Screened hybrid density functionals applied to solids" [J. Chem. Phys. 124, 154709 (2006)], J. Chem. Phys. 125 (2006) 249901.
[80] J. Heyd, G.E. Scuseria, M. Ernzerhof, Hybrid functionals based on a screened Coulomb potential, J. Chem. Phys. 118 (2003) 8207–8215.
[81] J. Heyd, G.E. Scuseria, M. Ernzerhof, Erratum: "Hybrid functionals based on a screened Coulomb potential" [J. Chem. Phys. 118, 8207 (2003)], J. Chem. Phys. 124 (2006) 219906.
[82] H.J. Monkhorst, J.D. Pack, Special points for Brillouin-zone integrations, Phys. Rev. B 13 (1976) 5188–5192.
[83] M. Pumera, C.H.A. Wong, Graphane and hydrogenated graphene, Chem. Soc. Rev. 42 (2013) 5987–5995.
[84] C.J. Rupp, S. Chakraborty, R. Ahuja, R.J. Baierle, The effect of impurities in ultra-thin hydrogenated silicene and germanene: a first principles study, Phys. Chem. Chem. Phys. 17 (2015) 22210–22216.
[85] W. Wei, Y. Dai, B. Huang, T. Jacob, Many-body effects in silicene, silicane, germanene and germanane, Phys. Chem. Chem. Phys. 15 (2013) 8789–8794.
[86] Q. Peng, S. De, Elastic limit of silicane, Nanoscale 6 (2014) 12071–12079.
[87] B. Delley, From molecules to solids with the DMol^3 approach, J. Chem. Phys. 113 (2000) 7756–7764.
[88] B. Delley, An all-electron numerical method for solving the local density functional for polyatomic molecules, J. Chem. Phys. 92 (1990) 508–517.
[89] H. Liu, A.T. Neal, Z. Zhu, Z. Luo, X. Xu, D. Tománek, P.D. Ye, Phosphorene: an unexplored 2D semiconductor with a high hole mobility, ACS Nano 8 (2014) 4033–4041.
[90] J. Jiang, Q. Liang, R. Meng, Q. Yang, C. Tan, X. Sun, X. Chen, Exploration of new ferromagnetic, semiconducting and biocompatible Nb_3X_8 (X = Cl, Br or I) monolayers with considerable visible and infrared light absorption, Nanoscale 9 (2017) 2992–3001.
[91] J.-A. Yan, S.-P. Gao, R. Stein, G. Coard, Tuning the electronic structure of silicene and germanene by biaxial strain and electric field, Phys. Rev. B 91 (2015) 245403.
[92] Y. Zhang, T.-T. Tang, C. Girit, Z. Hao, M.C. Martin, A. Zettl, M.F. Crommie, Y.R. Shen, F. Wang, Direct observation of a widely tunable bandgap in bilayer graphene, Nature 459 (2009) 820–823.
[93] Y. Li, S. Yang, J. Li, Modulation of the electronic properties of ultrathin black phosphorus by strain and electrical field, J. Phys. Chem. C 118 (2014) 23970–23976.
[94] B. Sahu, H. Min, A.H. MacDonald, S.K. Banerjee, Energy gaps, magnetism, and electric-field effects in bilayer graphene nanoribbons, Phys. Rev. B 78 (2008) 45404.
[95] Y. Song, X. Wang, W. Mi, Spin splitting and electric field modulated electron-hole pockets in antimonene nanoribbons, npj Quant. Mater. 2 (2017) 15.

Figure Captions

Fig. 1 (a) Crystal structure of chairlike silicane monolayer (top & side view). The blue and green balls denote Si and H atoms respectively. (b) Electronic band structure of pristine silicane monolayer computed using PBE functional. The zero energy value corresponds to the Fermi level. (c) The partial charge densities of the CBM (up) and VBM (down). The isovalue is 0.002 e/A^3.

Fig. 2 Crystal structure (left panel) and electronic band structure (right panel) of four silicane bilayer configurations: (a) AA, (b) AB, (c) AA', and (d) AB' computed using PBE functional. The zero energy value corresponds to the Fermi level. The binding energies are also given.

Fig. 3 (a) Crystal structure of silicane bilayer (top & side view). The blue and green balls denote Si and H atoms respectively. (b) Electronic band structure of silicane bilayer computed using PBE functional. The zero energy value corresponds to the Fermi level.

Fig. 4 Crystal structure (left panel) and electronic band structure (right panel) of: (a) silicane trilayer, and (b) silicane tetralayer, (c) silicane pentalayer and (d) bulk silicane computed using PBE functional. The blue and green balls denote Si and H atoms respectively. The zero energy value corresponds to the Fermi level.

Fig. 5 Electronic band structure under biaxial tensile strain of: (a) silicane monolayer and (b) silicane bilayer. The zero energy value corresponds to the Fermi level.

Fig. 6 Energy bandgap of silicane monolayer and bilayer as a function of the biaxial tensile strain computed using PBE functional.

Fig. 7 Energy bandgap of silicane monolayer and bilayer as a function of the external E-field computed using PBE functional.

Fig. 8 Electronic band structures of (a) silicane monolayer under the external E-field of 0.5 V/Å and (b) silicane bilayer under the external E-field of 0.7 V/Å computed using PBE functional. The zero energy value corresponds to the Fermi level.

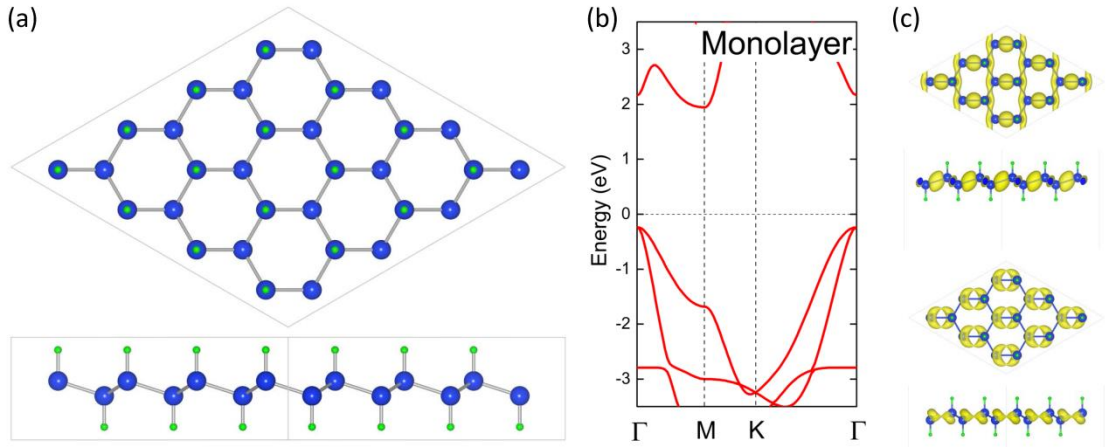

Fig. 1 (a) Crystal structure of chairlike silicane monolayer (top & side view). The blue and green balls denote Si and H atoms respectively. (b) Electronic band structure of pristine silicane monolayer computed using PBE functional. The zero energy value corresponds to the Fermi level. (c) The partial charge densities of the CBM (up) and VBM (down). The isovalue is 0.002 e/A^3.

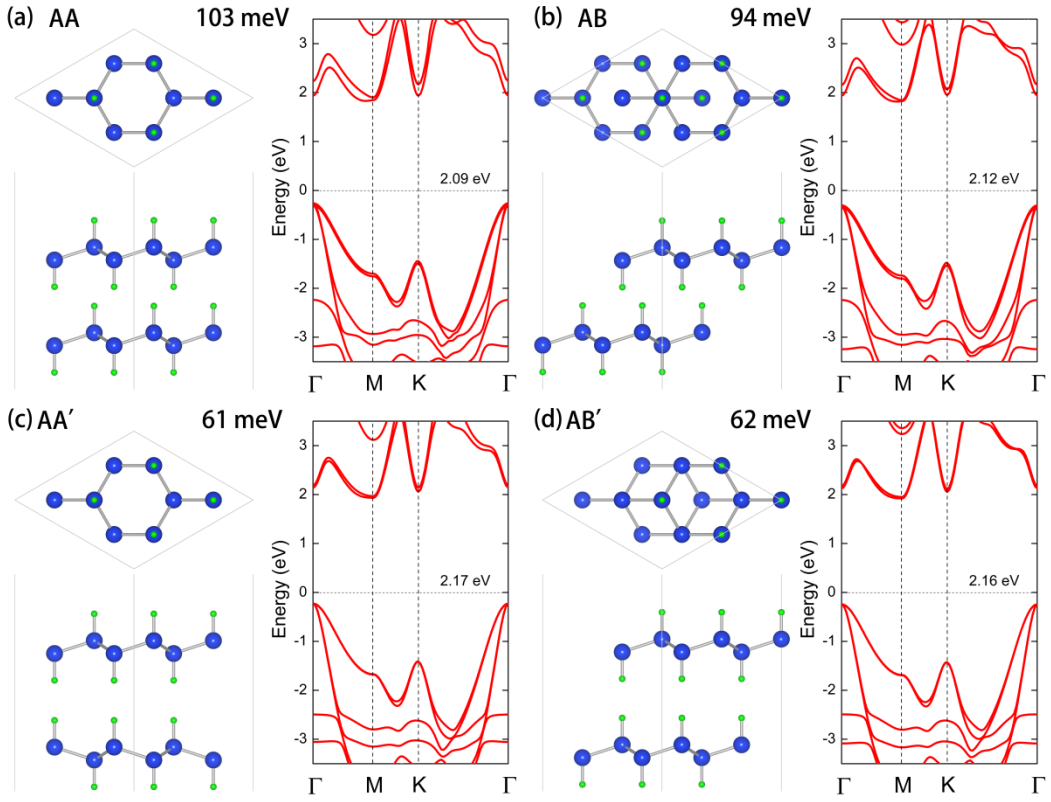

Fig. 2 Crystal structure (left panel) and electronic band structure (right panel) of four silicane bilayer configurations: (a) AA, (b) AB, (c) AA', and (d) AB' computed using PBE functional. The zero energy value corresponds to the Fermi level. The binding energies are also given.

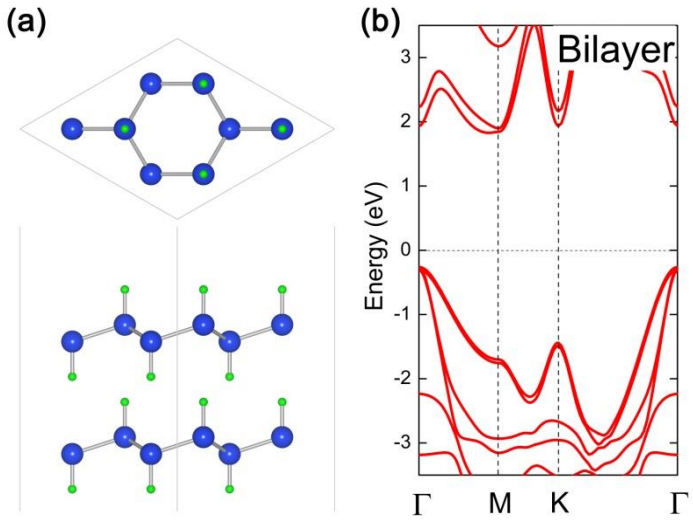

Fig. 3 (a) Crystal structure of silicane bilayer (top & side view). The blue and green balls denote Si and H atoms respectively. (b) Electronic band structure of silicane bilayer computed using PBE functional. The zero energy value corresponds to the Fermi level.

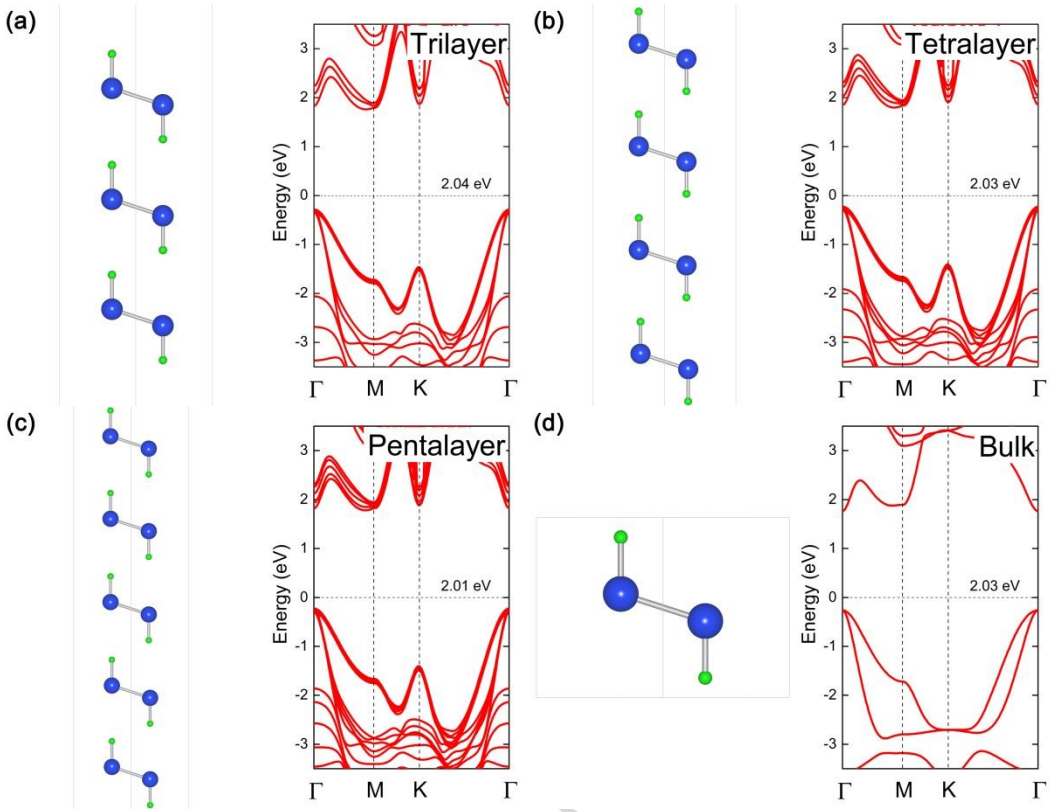

Fig. 4 Crystal structure (left panel) and electronic band structure (right panel) of: (a) silicane trilayer, and (b) silicane tetralayer, (c) silicane pentalayer and (d) bulk silicane computed using PBE functional. The blue and green balls denote Si and H atoms respectively. The zero energy value corresponds to the Fermi level.

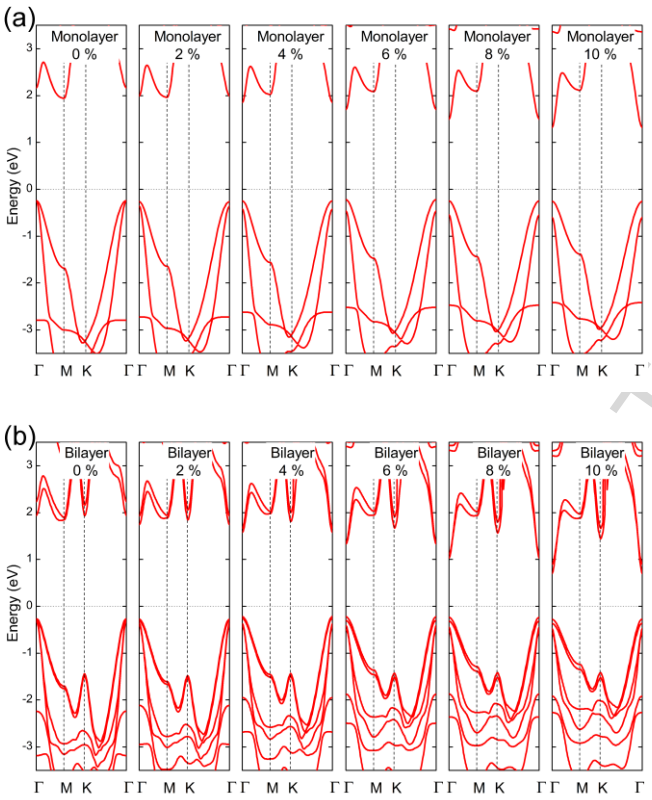

Fig. 5 Electronic band structure under biaxial tensile strain of: (a) silicane monolayer and (b) silicane bilayer. The zero energy value corresponds to the Fermi level.

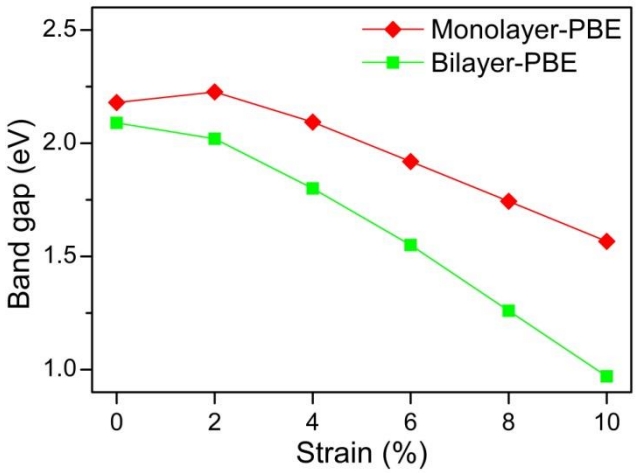

Fig. 6 Energy bandgap of silicane monolayer and bilayer as a function of the biaxial tensile strain computed using PBE functional.

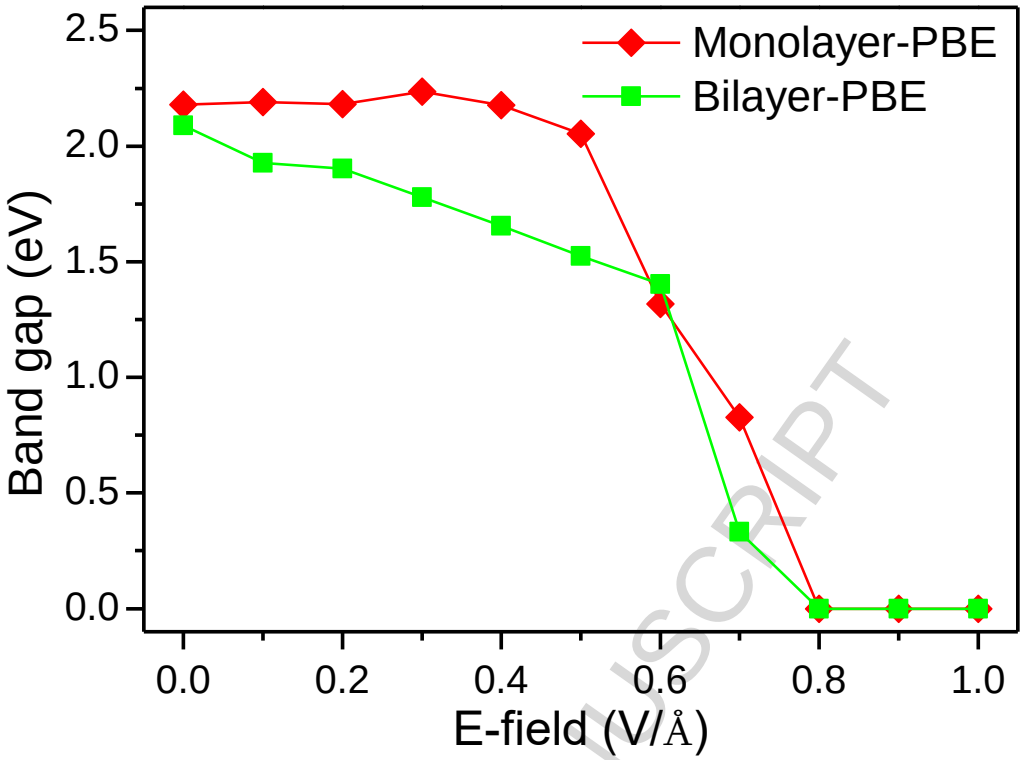

Fig. 7 Energy bandgap of silicane monolayer and bilayer as a function of the external E-field computed using PBE functional.

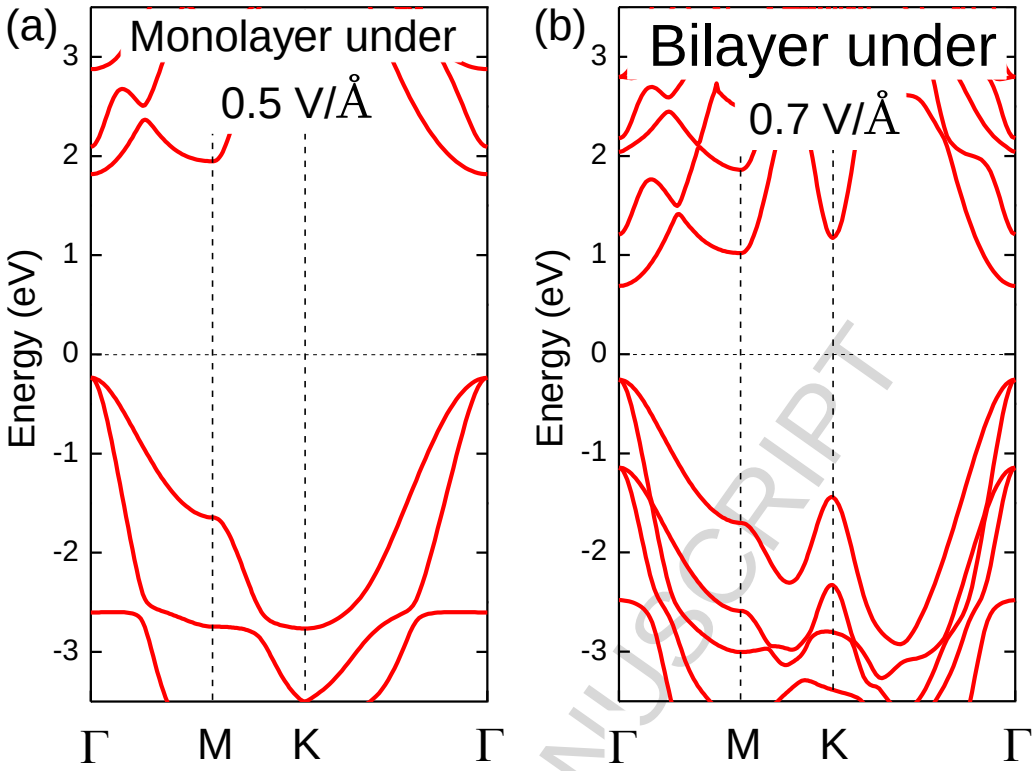

Fig. 8 Electronic band structures of (a) silicane monolayer under the external E-field of 0.5 V/Å and (b) silicane bilayer under the external E-field of 0.7 V/Å computed using PBE functional. The zero energy value corresponds to the Fermi level.

Highlights

1. The band gaps of silicane multilayers slightly decrease with the number of layers.
2. The bulk silicane is a direct band gap semiconductor.
3. The electric field can trigger an indirect-direct transition in silicane layers.